J Therm Anal Calorim (2012) 108:481–488
DOI 10.1007/s10973-011-2017-4

Phase diagram and electrical conductivity of the $DyBr_3$–RbBr binary system

I. Chojnacka · L. Rycerz · M. Berkani · M. Gaune-Escard

3rd Joint Czech-Hungarian-Polish-Slovak Thermoanalytical Conference Special Chapter

Abstract Phase equilibrium in the $DyBr_3$–RbBr binary system was established from differential scanning calorimetry measurements. This system exhibits three compounds, namely Rb_3DyBr_6, Rb_2DyBr_5, and $RbDy_2Br_7$, and two eutectics located at $DyBr_3$ molar fraction $x = 0.116$ ($T = 886$ K) and $x = 0.458$ ($T = 702$ K), respectively. Rb_3DyBr_6 undergoes a solid–solid phase transition at 726 K and melts congruently at 1,059 K. Rb_2DyBr_5 and $RbDy_2Br_7$ melt incongruently at 737 and 748 K, respectively. The electrical conductivity of $DyBr_3$–RbBr liquid mixtures was measured over the whole composition range. Results obtained are discussed in term of possible complex formation.

Keywords DSC · Phase diagram · Dysprosium bromide · Rubidium bromide · Electrical conductivity

I. Chojnacka · L. Rycerz (✉)
Chemical Metallurgy Group, Faculty of Chemistry, Wroclaw University of Technology, Wybrzeze Wyspianskiego 27, 50-370 Wroclaw, Poland
e-mail: leszek.rycerz@pwr.wroc.pl

M. Berkani
Laboratoire de Génie de l'Environnement, Département de Chimie, Faculté des Sciences Exactes, Université A. Mira, 06000 Béjaïa, Algérie

M. Gaune-Escard
Ecole Polytechnique, Mecanique Energetique, Technopole de Chateau-Gombert, 5 rue Enrico Fermi, 13453 Marseille Cedex 13, France

Introduction

Rare-earth halides are technologically important since they are used in a number of applications like recycling of spent nuclear fuel, reprocessing of nuclear waste, doses in high-intensity discharge lamps, new highly efficient light source with energy-saving features, lasers, and so forth. However, the thermodynamic data on their halide systems available in literature are scarce and it is not uncommon that the values appearing in reference tables come from estimation. In addition, experimental data in literature are often contradictory. All of the lanthanide–alkali metal chloride binary systems have been successfully examined or reexamined at large by Seifert [1]. The phase diagrams of the homologous bromide and iodide systems were not fully investigated nor critically assessed yet. Among the little information available, some lanthanide–alkali metal bromide systems seem totally erroneous: in the $TmBr_3$–RbBr system [2] for instance surprisingly no congruently melting compound has been reported, which is inconsistent with the general trends observed for all the LnX_3–RbX systems. Other systems were investigated [3], but resulted in mostly graphic-only information. Therefore, more details would be required to fully characterize those systems. Taking into account the above discrepancies or lack of data for many $LnBr_3$-based binary systems, we decided to assess existing data and to investigate the still unexplored lanthanide bromide-based systems. These data are also crucial for modeling of thermodynamic properties or to prediction of the thermodynamic data of other lanthanide halide-based systems [4–6].

This article is a part of our ongoing extensive program focused on thermodynamic properties, structure, and electrical conductivity of LnX_3–MX systems. It reports the thermodynamic and transport properties of $DyBr_3$–RbBr

binary system. The only literature information on this system was the graphic form of the phase diagram reported by Blachnik and Jaeger-Kasper [3].

Experimental

Chemicals and samples preparation

Dysprosium(III) bromide was synthesized from the dysprosium(III) oxide (Sigma-Aldrich, min. 99.9%). This oxide was dissolved in hot concentrated hydrobromic acid. Solution was evaporated and $DyBr_3 \cdot xH_2O$ was crystallized and dried gradually at 380 and 410 K. Ammonium bromide was then added and this mixture was first slowly heated up to 450 K and then up to 570 K to remove the water. Resulting mixture was subsequently heated to 720 K for sublimation of NH_4Br. Finally, the salt was melted at 1,270 K. Crude $DyBr_3$ was purified by distillation under reduced pressure (10^{-3} Pa) in a quartz ampoule at 1,320 K. Chemical analysis was performed by complexometric (dysprosium) and mercurometric (bromide) methods. The results were as follows: Dy: 40.37 ± 0.12% (40.40% theoretical); Br: 59.61 ± 0.13% (59.60% theoretical).

Rubidium bromide was Alfa Aesar reagent (min. 99,9%). Before use, it was dried at 470 K.

The mixtures of $DyBr_3$ and RbBr (in appropriate proportions weighed with precision of about 1 mg) were melted in vacuum-sealed quartz ampoules in an electric furnace. Melts were homogenized by shaking and solidified. These samples were ground in an agate mortar in a glove box. Homogeneous mixtures of different composition prepared along the sample procedure were used both in phase diagram and electrical conductivity measurements. Although only a small amount of samples were used for the differential scanning calorimetry (DSC) experiments (200–400 mg), 2–3 g of each sample were synthesized in order to avoid deviation from stoichiometry.

All chemicals were handled in an argon glove box with a measured water content of about 2 ppm (V) and continuous gas purification by forced recirculation through external molecular sieves.

Measurements

Setaram DSC 121 was used to investigate phase equilibrium in the $DyBr_3$–RbBr system. Experimental samples (200–400 mg) were contained in vacuum-sealed quartz ampoules (about 6 mm diameter, 15 mm length). Measurements were conducted at heating and cooling rates ranging between 1 and 5 K min^{-1}. Because of the temperature limitation of DSC 121 (1,100 K), liquidus temperatures of mixtures reach in $DyBr_3$ were determined with the Paulik-Erdey thermal analyzer. Liquidus temperatures were determined as temperatures corresponding to the related peaks maximum. In all other cases, onset temperature (T_{ons}) was determined as effect temperature. DSC experiments were performed two times for several samples in order to analyze accuracy and repeatability of measurements. Difference in thermal effects temperature was significantly less than 1 K (usually 0.1–0.2 K) for the same sample.

Electrical conductivity measurements were carried out in the capillary quartz cell described in details elsewhere [7], and calibrated with molten NaBr [8]. The conductivity of the melt was measured by platinum electrodes with the conductivity meter Tacussel CDM230 during increasing and decreasing temperature runs. The mean values of these two runs were used in calculations. Experimental runs were performed at heating and cooling rates of 2 K min^{-1}. Temperature was measured with a Pt/Pt–Rh(10) thermocouple with 1 K accuracy. Temperature and conductivity data acquisition were made with PC computer, interfaced to the conductivity meter. All measurements were carried out under static argon atmosphere. The accuracy of the measurements was about ±2%.

Results and discussion

Phase diagram

The DSC investigations were performed on samples with different compositions yielded both the corresponding temperature and enthalpy values. Due to noticeable supercooling effect occurring during cooling runs, all experimental temperature and enthalpy data were determined from heating curves. Heating rate of 5 K min^{-1} was used to determine temperature of thermal effects. However, due to overlapping of peaks, lower heating rates (up to 1 K min^{-1}) had to be used in order to separate these effects and obtain precise enthalpy values. Figure 1 shows the thermograms for samples with molar fraction of $DyBr_3$, $x = 0.075$ (a), 0.283 (b), 0.376 (c), 0.472 (d), 0.609 (e), and 0.706 (f), obtained with heating rate of 5 K min^{-1}. In all the thermograms, the endothermic effect at the highest temperature corresponds to liquidus and its temperature was determined as peak maximum temperature.

In the composition range $0 < x < 0.25$, where x is the molar fraction of $DyBr_3$, two additional endothermic peaks were present in all heating thermograms (Fig. 1a). The first one, at 886 K (mean value for all samples), is observable up to $x = 0.250$, where it disappeared, thus suggesting the existence of a compound with the stoichiometry of Rb_3DyBr_6. This thermal event at 886 K can be undoubtedly ascribed to the RbBr–Rb_3DyBr_6 eutectic. The second

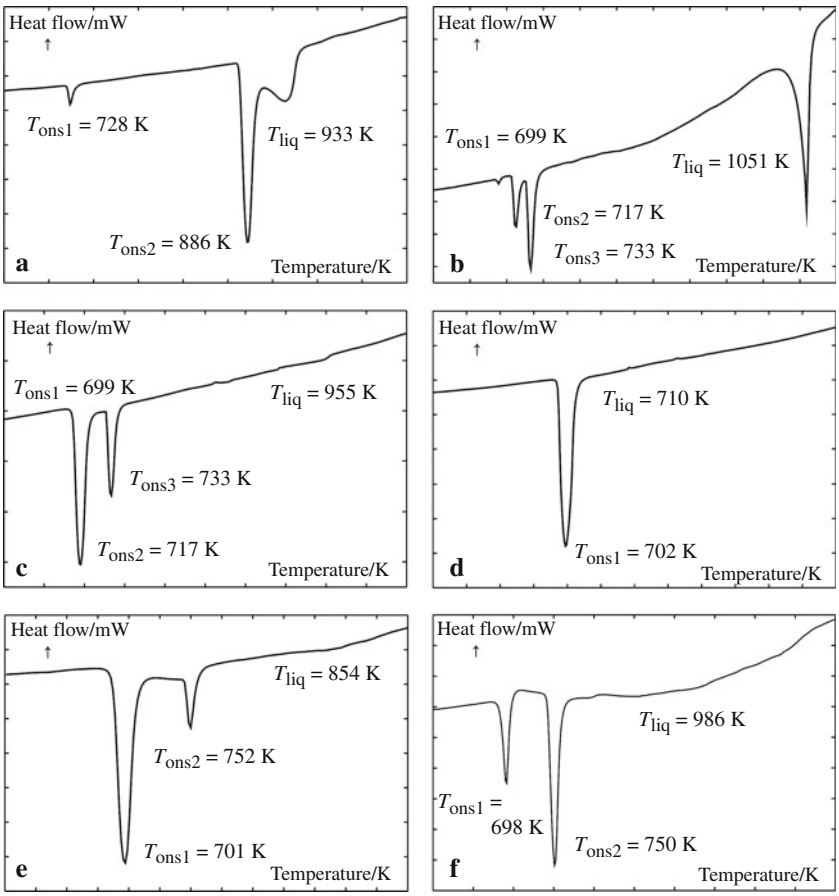

Fig. 1 DSC heating curves for $DyBr_3$–RbBr mixtures of different compositions: **a** $x = 0.075$, **b** $x = 0.283$, **c** $x = 0.376$, **d** $x = 0.472$, **e** $x = 0.609$, **f** $x = 0.706$. Heating rate—5 K min^{-1}

effect at 726 K could correspond to the solid–solid phase transition of Rb_3DyBr_6 compound. In such situation it should appear also in the samples with x bigger than 0.250. However, in the composition range $0.25 < x < 0.40$ (Fig. 1b, c), three endothermic peaks were present in addition to liquidus (at temperatures 700, 717, and 734 K), not any of them corresponds to the temperature 726 K. It seemed very likely that another, incongruently melting Rb_2DyBr_5 compound exists in the system under investigation. Its existence could cause a typical difficulty for the investigations of phase diagrams with incongruently melting compounds [9]. Because of the large temperature difference of the melting point of Rb_3DyBr_6 (1,059 K) and the potential eutectic formed by Rb_2DyBr_5 compound (about 700 K) during cooling a large amount of Rb_3DyBr_6 crystallizes from the melt above the temperature incongruent melting of Rb_2DyBr_5 (presumably 734 K). The crystals separate from the melt and, therefore, the formation of Rb_2DyBr_5 is not complete. As a consequence, all other effects at lower temperatures, namely the eutectic and phase transition of Rb_3DyBr_6 will appear also in the range of compositions where mentioned above temperature difference is large. Thus, the quenched samples have to be annealed to get equilibrium conditions [9]. We have performed the annealing of the samples with molar fraction of the $DyBr_3$ ranging from 0.25 to 0.40 at temperature of 708 K during 78 h. The thermograms of the samples with $x = 0.283$ and $x = 0.376$ without annealing and after annealing, obtained with heating rate 1 K min^{-1}, are presented in Fig. 2. For the samples with molar fraction $x < 0.333$ effect at about 700 K (potentially related to the Rb_2DyBr_5 eutectic disappears (Fig. 2a, b). For the samples with molar fraction $x > 0.333$ disappears effect at temperature of about 717 K (Fig. 2c, d) corresponding to the phase transition of Rb_3DyBr_6. These annealing experiments confirmed existence of incongruently melting at 737 K (mean value from all appropriate thermograms) Rb_2DyBr_5 compound. Effect at lower temperature (702 K) is related to the eutectic formed by Rb_2DyBr_5.

In the composition range $0.50 < x < 1.00$, two endothermic peaks were present in all heating thermograms in addition to liquidus (Fig. 1e, f). The temperature of first effect correspond very well with effect observed for samples with molar fraction of $DyBr_3$ $0.25 < x < 0.50$ (about 702 K). The second effect occurs at about 750 K and suggests existence of another incongruently melting compound. However, existence of this compound should influence effect at lower temperature (702 K). At

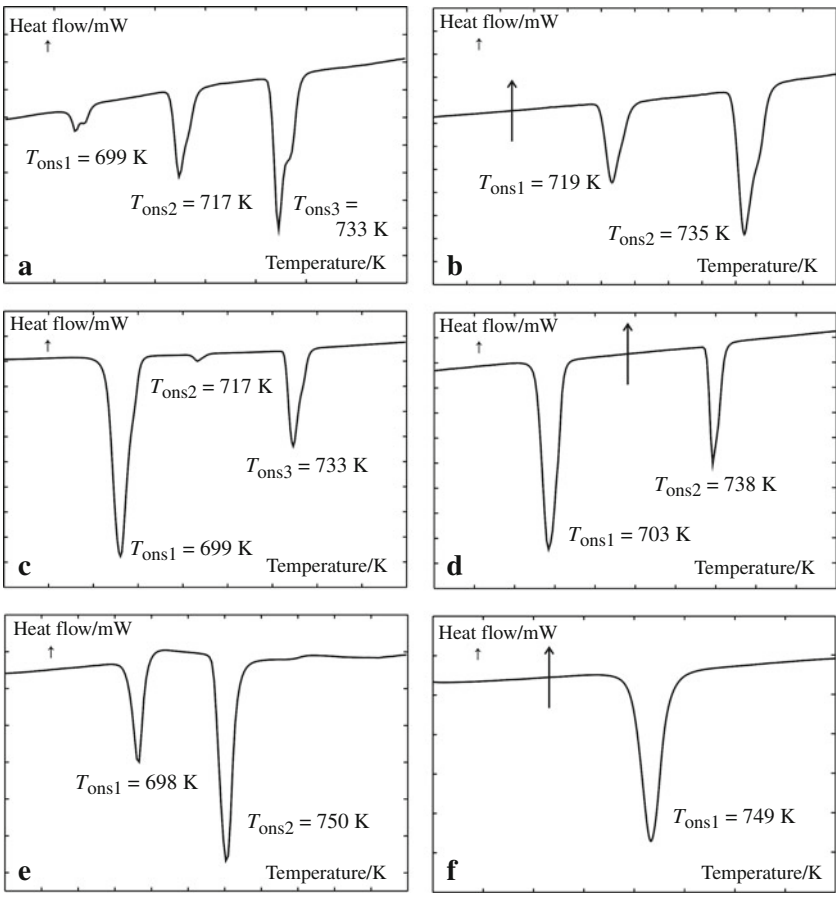

Fig. 2 DSC heating curves for $DyBr_3$–RbBr without (**a**, **c**, **e**) and after (**b**, **d**, **f**) annealing at 708 K during 48 h: **a**, **b** $x = 0.283$; **c**, **d** $x = 0.376$; **e**, **f** $x = 0.706$. Heating rate—1 K min^{-1}

composition of this compound effect at 702 K, related to the eutectic, should disappear. But once again we have the situation of large difference between melting temperature of $DyBr_3$ (1,152 K) and temperature of incongruent melting of this hypothetical compound (750 K). Annealing of the samples was performed at 708 K during 78 h. As a result of this annealing the thermal effect at 702 K disappeared in the samples with $x > 0.666$ (Fig. 2e, f), thus, suggesting existence of $RbDy_2Br_7$ incongruently melting compound.

In the composition range $x > 0.80$, an additional effect at about 479 K was observed. It is related to the phase transition of $DyBr_3$.

For all effects (with exception of liquidus), the Tamman plots (experimental enthalpy per mole of mixture vs. $DyBr_3$ mol fraction) were constructed (Fig. 3) in order to determine eutectics composition and stoichiometry of definite compounds that exist in the system. The RbBr–Rb_3DyBr_6 and Rb_2DyBr_5–$RbDy_2Br_7$ eutectic composition found to be $x = 0.116$ and 0.458, respectively. (Figure 3a, b). The corresponding eutectic temperatures (determined as mean value) are 886 and 702 K, respectively. Stoichiometry of Rb_2DyBr_5 and $RbDy_2Br_7$ determined from Tamman diagrams (Fig. 3d, e, respectively) constructed for their incongruent melting effects was found to be 0.322 and 0.689. These values are in quite good agreement with theoretical values (0.333 and 0.666, respectively).

All the results of DSC investigations are presented in Table 1, and the complete phase diagram is shown in Fig. 4. Our results could be compared with existing

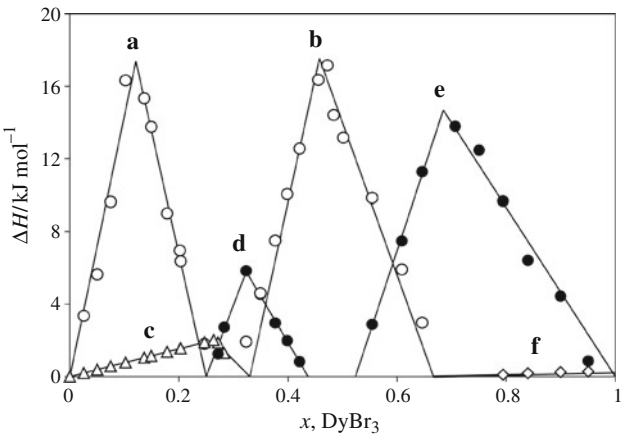

Fig. 3 Tamman plot of $DyBr_3$–RbBr binary system: determination of: *a* (*open circles*) RbBr–Rb_3DyBr_6 and *b* (*open circles*) Rb_2DyBr_5–$RbDy_2Br_7$ eutectic composition; stoichiometry determination of: *c* (*open triangles*) Rb_3DyBr_6, *d* (*filled circles*) Rb_2DyBr_5 and *e* (*filled circles*) $RbDy_2Br_7$ compound; *f* (*open diamonds*) $DyBr_3$ phase transition

Table 1 DSC final results for $DyBr_3$–RbBr binary system

x ($DyBr_3$)	T/K						
	RbBr–Rb_3DyBr_6 eutectic	Rb_3DyBr_6 transition	$Rb_3Dy_2Br_9$ decomposition	$Rb_3Dy_2Br_9$–$DyBr_3$ eutectic	$RbDy_2Br_7$ decomposition	$DyBr_3$ decomposition	Liquidus
0							966
0.026	887	727					–
0.050	885	726					947
0.075	886	728					933
0.102	886	727					–
0.136	887	728					–
0.149	886	728					943
0.178	885	727					975
0.202	887	727					1019
0.203	885	727					1017
0.247	887	728					1053
0.272		719	735				1054
0.283		719	735				1051
0.323			737	702			1002
0.349			738	703			952
0.376			738	703			955
0.398			738	703			891
0.421			738	703			776
0.456				702			707
0.472				702			710
0.484				703			755
0.501				702			739
0.554				703	753		816
0.609				701	752		854
0.646				701	752		936
0.706					749		986
0.750					747		1017
0.794					748	479	1047
0.840					746	480	1075
0.900					746	479	1114
0.950					743	479	1133
1						488	1152

literature data [3] presented in graphic form only. We have estimated from this graphic form both the temperatures and compositions of characteristic points. The same compounds, namely Rb_3DrBr_6, Rb_2DyBr_5, and $RbDy_2Br_7$ were found to exist in the system. In both cases, Rb_3DrBr_6 undergoes the solid–solid phase transitions and melts congruently at temperatures 726 and 1,059 K (our results) and 727 and 1,056 K (literature data), respectively. $RbDy_2Br_7$ melts incongruently at 748 K (our results and literature data). In the case of Rb_2DyBr_5, significant difference could be observed. According to our findings, this compounds melts incongruently at temperature 737 K, i.e., at temperature higher than temperature of solid–solid phase transition of Rb_3DrBr_6 compound. According literature data [3], it melts incongruently at temperature of about 719 K, i.e., temperature lower than temperature of solid–solid phase transition of Rb_3DrBr_6 compound. As a consequence, different composition ranges of the existence of Rb_3DrBr_6 solid–solid phase transition could be observed. According to our findings, this transition appears only up to molar fraction of $DyBr_3$ equal 0.333, whereas according to [3], this molar fraction of $DyBr_3$ is significantly larger (of about 0.5). Some differences as well as similarities were found also in the case of RbBr-Rb_3DrBr_6 and Rb_2DyBr_5–$RbDy_2Br_7$ eutectics. The excellent agreement was found for the RbBr–Rb_3DyBr_6 eutectic temperature (886 and

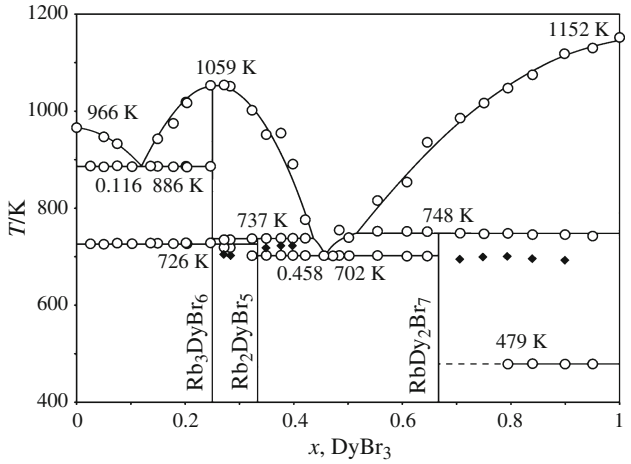

Fig. 4 Phase diagram of the $DyBr_3$–RbBr binary system: *filled diamond* additional effects in samples without annealing

885 K, respectively). However, our finding for eutectic composition ($x = 0.116$) differ from literature data (of about 0.15). In the case of Rb_2DyBr_5–$RbDy_2Br_7$ eutectic, quite good agreement was found for eutectic composition 0.458 and of about 0.45 [3]), while determined by us eutectic temperature is insensibly larger in comparison with cited literature (702 and 689 K, respectively).

Electrical conductivity

The electrical conductivity of the $DyBr_3$–RbBr liquid mixtures was measured for the first time. Experimental determinations were conducted over the entire composition range in steps of about 10%.

The experimental conductivity, κ, data of the liquid phase were fitted to the second-order equation against temperature (T):

$$\ln \kappa = A_0 + A_1(1000/T) + A_2(1000/T)^2 \quad (1)$$

where A_0, A_1, and A_2 are coefficients determined by the least-squares method. The activation energy, E_A, evaluated by analogy to the Arrhenius equation as:

$$E_A(T) = -R\mathrm{d}\ \ln(\kappa)/\mathrm{d}(1000/T) \quad (2)$$

where R is the gas constant, becomes:

$$E_A(T) = -R[A_1 + 2A_2(1000/T)] \quad (3)$$

All A_i coefficients are listed in Table 2, together with the E_A values determined at 1,180 K (at this temperature, all the mixtures independently on composition, are liquid) for all of the $DyBr_3$–RbBr mixtures.

The experimental conductivity isotherm at 1,180 K was plotted against the molar fraction of $DyBr_3$ in Fig. 5. Conductivity decreases with increase of $DyBr_3$ concentration, with significantly larger changes in the rubidium

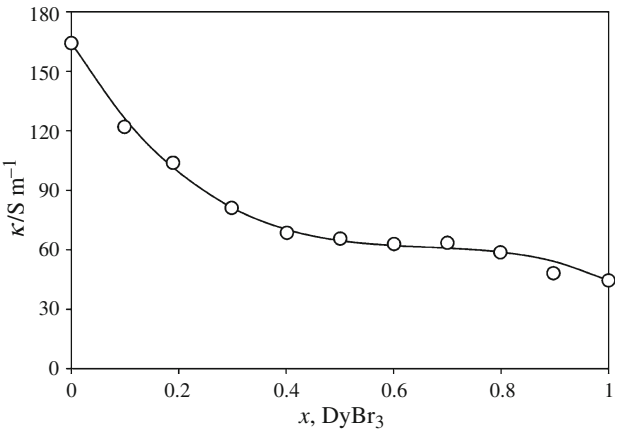

Fig. 5 Electrical conductivity isotherm of $DyBr_3$–RbBr liquid mixtures at 1,180 K

Table 2 Coefficients in equation: $\ln \kappa = A_0 + A_1(1000/T) + A_2(1000/T)^2$ and activation energy of the electrical conductivity (E_A) of $DyBr_3$–RbBr liquid mixtures at 1,180 K: κ in $S{\cdot}m^{-1}$, ln(s) standard deviation of ln κ, n number of experimental data points

x ($DyBr_3$)	Temperature range/K	A_0/S m^{-1}	A_1/S m^{-1} K	A_2/S m^{-1} K^2	ln(s)	n	E_A at 1,180 K/kJ mol^{-1}
0.000	1080–1270	4.5625	2.3488	−2.0214	0.0972	241	8.9568
0.099	1080–1270	4.8844	1.2317	−1.5658	0.0896	257	11.824
0.189	1080–1270	4.6416	1.7597	−2.0741	0.0714	246	14.597
0.298	1080–1270	3.7280	3.7142	−3.4524	0.0751	270	17.770
0.401	1080–1270	6.3073	−2.2943	−0.1877	0.0988	247	21.720
0.500	1080–1270	2.6165	6.3251	−5.2808	0.1261	256	21.828
0.598	1090–1270	−7.5628	30.292	−19.447	0.1815	257	22.190
0.700	1160–1240	4.4948	1.4176	−2.1516	0.1378	196	18.534
0.799	1200–1310	3.5495	4.0684	−4.0728	0.1006	157	23.568
0.897	1140–1240	4.1009	2.5036	−3.2682	0.0954	136	25.239
1.000	1140–1270	3.9420	3.5616	−4.4061	0.1047	234	32.478

bromide-rich region. Decrease of RbBr molar fraction causes decrease of the mobile ion number (Rb^+, Br^-), which are carries of electrical charge and results in decrease of specific conductivity. A similar trend has been observed in our previous investigations of lanthanide halide–alkali metal halide binary systems [10–12].

In many cases, the composition dependence of specific conductivity of binary mixtures can be well represented by Kuroda [13] equation:

$$\kappa_{\text{Kuroda}} = x_1^2\kappa_1 + x_2^2\kappa_2 + 2x_1x_2\kappa_1 \quad (4)$$

where x_1 and x_2 are the molar fraction of the pure components, and κ_1 and κ_2 are their specific conductivities, with $\kappa_1 < \kappa_2$. However, in the case of the liquid mixtures investigated here, significant negative deviations of experimental results from this equation were observed. These relative deviations, calculated from Eq. 5, are presented in the Fig. 6.

$$\Delta\kappa = \frac{\kappa_{\text{exp}} - \kappa_{\text{Kuroda}}}{\kappa_{\text{Kuroda}}} \times 100\% \quad (5)$$

According to literature [14], negative electrical conductivity deviations are strongly indicative of complex formation. If only one complex species exists in the melt, the absolute value of deviation reaches a maximum at the composition corresponding to the stoichiometry of this complex. If several complex species co-exist, the location of the minimum may slightly deviate from the exact stoichiometry of the predominant species. Raman spectroscopic investigations [15] showed that octahedral $LnBr_6^{3-}$ complex ions are formed in the $LnBr_3$–MBr liquid mixtures. These $LnBr_6^{3-}$ complex ions constitute indeed the predominant species in the MBr-rich liquid mixtures. As the $LnBr_3$ concentration increases, a distortion of these octahedra occurs. Distorted octahedra are bridged through bromide anions. The formation of $LaBr_6^{3-}$ complex ions should be reflected in the electrical conductivity plot versus composition. Experimental results (Fig. 6) show a broad minimum on the deviation curve located at dysprosium bromide molar fraction $x \approx 0.30$–0.35. The shift of the negative conductivity minimum from 25% $DyBr_3$ (composition that would correspond to the $DyBr_6^{3-}$ single complex species) toward a richer composition is consistent with the structural conclusion [15] that $DyBr_6^{3-}$ octahedra may generate and coexist with polymeric units of the same. Therefore, the existence of negative deviations in $DyBr_3$–RbBr liquid mixtures with a minimum at $x \approx 0.30$–0.35 is indicative of $DyBr_6^{3-}$ octahedral complex formation in the melt.

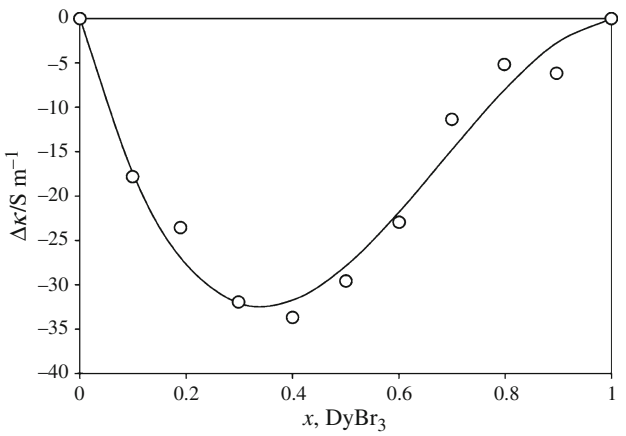

Fig. 6 Relative deviation of the electrical conductivity at 1,180 K from the Kuroda equation (4) for $DyBr_3$–RbBr liquid mixtures

Activation energy for electrical conductivity at 1,180 K as function of the composition for $DyBr_3$–RbBr system is presented in Table 2. It increases up to about 40 mol% of $DyBr_3$ and become almost stable up to 80 mol% of $DyBr_3$. This plateau can be explained in terms of coexistence of different forms of complexes (polymeric form of $DyBr_6^{3-}$ octahedral).

Conclusions

1. Differential scanning calorimetry is a very useful tool for phase diagram determination.
2. Precise data on enthalpy of thermal effects give possibility of correct determination of eutectics and incongruently melting compounds stoichiometry with using the Tamman diagrams.
3. A typical difficulty for the investigations of phase diagrams with incongruently melting compounds arose also in the system under investigation and quenched samples have to be annealed to get equilibrium conditions.
4. The electrical conductivity of $DyBr_3$–RbBr liquid mixtures measured over an extended temperature range and on the whole composition range is indicative of octahedral $DyBr_6^{3-}$ complexes formation.

Acknowledgements Financial support by Polish Ministry of Science and Higher Education from budget on science in 20070-2010 under the Grant No. N204 4098 33 and by the Department of Chemistry of Wroclaw University of Technology from budget on science in 2011 under the grant 344120/Z310 is gratefully acknowledged. I.Ch. and L.R. wish to thank the Ecole Polytechnique de Marseille for hospitality and support during this study. Studies co-financed by EU under the European Social Fund.

References

1. Seifert HJ. Thernary chlorides of the trivalent late lanthanides. J Therm Anal Calorim. 2006;83(2):479–505 and references therein.

2. Molodkin AK, Karagodina AM, Dudareva AG, Strekachinskii AB. $TmBr_3$–RbBr system. Zh Noerg Khim. 1981;26(8):2265–7.
3. Blachnik R, Jaeger-Kasper A. Zustandsdiagramme von alkali-bromid-lanthanoid(iii)-bromid-mischungen. Z Anorg Allg Chem. 1980;461:74–86.
4. Kapala J, Rutkowska I, Chojnacka I, Gaune-Escard M. Modelling of the thermodynamic properties of the ABr–$CeBr_3$ (A = Li-Cs) systems. CALPHAD. 2010;34:15–9.
5. Kapala J. Modelling of thermodynamic properties of ABr–$PrBr_3$ (A = Li-Cs) systems. CALPHAD. 2011;35:219–23.
6. Kapala J, Bochynska M, Broczkowska K, Rutkowska I. Prediction of the thermodynamic data of the pseudobinary alkali halide-lanthanide halide condensed systems. J Alloys Comp. 2008;451:679–81.
7. Fouque Y, Gaune-Escard M, Szczepaniak W, Bogacz A. Syntheses, mesures des conductibilities electriques et des entropie de changements d'etat pour le compose Na_2UBr_6. J Chim Phys. 1978;75:360–4.
8. Janz GI. Thermodynamic and transport properties for molten salts; correlation equations for critically evaluated density, surface tension, electrical conductance, and viscosity data. J Phys Chem Ref Data. 1988;2:17.
9. Sebastian J, Seifert HJ. Ternary chlorides in the systems ACl/YbCl3 (A.Cs, Rb, K). Thermochim Acta. 1998;318:29–37.
10. Gdzuric S, Ingier-Stocka E, Rycerz L, Gaune-Escard M. Electrical conductivity of molten binary $NdBr_3$-alkali bromide mixtures. Z Naturforsch. 2004;59a:77–83.
11. Ziolek B, Rycerz L, Gadzuric S, Ingier-Stocka E, Gaune-Escard M. Electrical conductivity of molten $LaBr_3$ and $LaBr_3$-MBr binary mixtures. Z Naturforsch. 2005;60a:75–80.
12. Ingier-Stocka E, Rycerz L, Gadzuric S, Gaune-Escard M. Thermal and conductometric studies of the $CeBr_3$–MBr binary systems (M = Li, Na). J Alloys Comp. 2008;450:162–6.
13. Mochinaga J, Cho K, Kuroda T. Denki Kagaku. 1968;36:746.
14. YuK Delimarskii, Markov BF. Electrochemistry of fused salts. Washington, DC: The Sigma press Publishers; 1961.
15. Photiadis GM, Borresen B, Papatheodorou GN. Vibrational modes and structures of lanthanide halide–alkali halide binary melts; $LnBr_3$–KBr (Ln = La, Nd, Gd) and $NdCl_3$–ACl (A = Li, Na, K, Cs). J Chem Soc Faraday Trans. 1998;17:2605–13.